

MODELLING MAGNETIC MATERIAL IMAGES WITH SIMULTANEOUS AUTOREGRESSIONS

Changjing Shang and D. M. Titterington

Department of Statistics
University of Glasgow
Glasgow G12 8QQ, UK
{shang, mike}@stats.gla.ac.uk

ABSTRACT

This paper presents a novel application of Simultaneous Autoregressive models to the synthesis of magnetic material images. The effects of using either symmetric or non-symmetric neighbour sets upon the visual and statistical properties of the resulting synthesised images are investigated. The use of a neighbour set whose shape corresponds to the orientations and coarseness of the texture allows the generation of synthetic images of good quality. Also, the size of such a neighbour set is usually smaller than that of the symmetric set required to reach similar modelling accuracy, thereby minimising the computational effort.

1. INTRODUCTION

Many new magnetic materials (MM) are currently under investigation for use in the ever-growing information storage industry [7], and important aspects of their properties can be gleaned from their texture images, which are obtained under different magnetic field strengths and direction angles by the use of Transmission Electron Microscopes. It is, therefore, of considerable practical interest to be able to produce model-based artificial MM images that will provide (i) a compact way of describing the textures observed experimentally and (ii) a source of insight into the factors controlling the textural ripple, from studies of the structure and parameters of the best fitting models.

Much of the existing work on the statistical modelling of images has involved Markov Random Field (MRF) models [1, 11, 12], and in particular the simultaneous autoregressive (SAR) model [4, 6, 10]. This is because the equivalent MRF representation of a given SAR model is characterised by more parameters, and the study of SAR models can be extended to include other simultaneous models which are not subsets of Markov models [4]. This paper therefore concentrates on the use of SAR models for MM image synthesis.

With SAR models it is important to choose an appropriate neighbourhood structure. Most approaches in the literature use prescribed fixed-size neighbour sets that are spatially symmetric, with little if any justification. We investigate the use of non-symmetric neighbour sets which reflect the underlying orientations

of the textures of interest. We compare the performances of different SAR models using the content similarity based approach [8, 9].

2. SAR MODELS

An observed (MM) image $Y = \{y(s)\}$ is assumed to be a random field defined on an $M \times M$ lattice Ω , where $y(s)$ denotes the grey level of a pixel at location $s = (i, j)$, $i, j = 0, 1, 2, \dots, M - 1$. Also, it is assumed to be stationary, i.e. $E[y(s)] = a$ with a being a constant. For any site s a neighbour set N is defined. The neighbour set of a pixel at or near the boundary of an image is defined by imposing a toroidal lattice structure [4]. The SAR model, expressed as follows, reflects the fact that the grey level at a site is associated with the grey levels of its neighbours [4, 6]:

$$y(s) = \sum_{r \in N} \theta_r y(s \oplus r) + \sqrt{\rho} w(s), \quad s \in \Omega.$$

Here, θ_r , $r \in N$, are the model parameters characterising the dependence of a pixel on its neighbours; $\{w(s)\}$ is Gaussian white noise with unit variance; ρ denotes the noise variance; and \oplus denotes an operator for addition modulo M in each coordinate.

Given an SAR model, a texture image can be synthesised by (a) choosing a neighbour set, and (b) estimating the values of the model parameters θ_r and ρ . A conventional least squares (LSQ) or maximum likelihood (ML) estimation algorithm can be used for (b); for details of these and the routine for simulating SAR realisations see [4, 6]. Although it is well known that LSQ can produce non-consistent estimators for SAR models [4], we tried both methods, in the knowledge that our MM images are, after all, not true realisations of the models.

3. SELECTION OF NEIGHBOUR SETS

Symmetric neighbour sets such as square shaped ones are usually used with SAR or MRF models [1, 6, 13], but the MM images have rather particular textural characteristics. In displaying the process of magnetic field reversal, they reveal strong directed ripples, and our experience with symmetric neighbour sets, even of a moderate size, e.g. 13×13 pixels, typically did not produce SAR models that fitted the data well, as we shall see.

Although one might consider fitting SAR models with randomly generated non-symmetric neighbour sets until a suitable one is found, the MM images tend to show one or more strong

This research is supported by UK EPSRC grant GR/K73114. The authors are grateful to Professor J. N. Chapman and Mr. Jason King for providing real microscopy images for use in this work, and to them and to Professor I. S. Molchanov for helpful discussions.

orientations, and this should be exploited. Our heuristic search approach for useful neighbour sets was as follows. Given an original image, it is first carefully examined to identify its distinctive texture shapes. The underlying orientation properties are then abstracted to form the shapes that are subsequently used to constrain the search. That is, when considering neighbour sets of a particular size (i.e. number of pixels), only those which satisfy at least one of the identified shapes are selected. As a result, only a few neighbour sets are tested. Moreover, it turns out that an upper limit on the sizes of the neighbour sets can be imposed. This enables good neighbour sets to be found with limited computational effort, and creates much better synthesised images than those based on symmetric neighbour sets.

4. RETRIEVAL OF SYNTHESISED IMAGES

The content similarity based retrieval technique is used to select the best models. The technique was originally developed to retrieve, from a given image database, those images that have the same or very similar characteristics to those specified in a user query [8, 9]. To reduce the computational complexity, low-level statistical features are used to represent images when performing the retrieval. In our application, the “user query” stands for the original image and the “image database” consists of a corresponding set of synthesised textures. The image features used to effect the comparisons are computed using a non-overlapping moving window, and include: (a) local *mean*, *standard deviation* and *skewness* features; (b) *gradient* features, computed by averaging the gradient values measured in the horizontal and vertical directions using the Sobel operators [2]; (c) *fractal* features, measured along horizontal, 45° diagonal, vertical and 135° diagonal directions [5]; and (d) *position* features, determined by the coordinates at the centre of the moving window.

In order to avoid biasing towards particular feature ranges the features are normalised to zero mean and unit standard deviation. The synthesised images are ranked on the basis of the Euclidean distance between the features of the original and those of the synthetic image, via a process of nearest-neighbour search [3].

5. SIMULATION RESULTS

The work reported here focuses on a particular type of MM image pertaining to the reversal of the free-layer in a permalloy-based spin-valve [7]. Nine real MM images of a size of 128×128 with the grey levels ranging from 0 to 255 are used in this study (Fig. 1). Although these images are taken from the same area of magnetic material, they have different visual properties, because of the use of magnetic fields of different magnitudes. All MM images present a smooth, rippling texture with marked directionalities.

5.1. Synthesis with Square-Shaped Neighbour Sets

Models were fitted based on five square-shaped neighbour sets, of sizes 3×3 , 5×5 , 7×7 , 9×9 and 13×13 , and in each case model parameters are estimated using both the LSQ and ML algorithms. Thus, for each original image ten (5×2) synthetic images, of a size of 128×128 , are generated. The method of Section 4 led to the 9 top ranked synthesised images, one per original, presented in Fig. 2. The caption indicates the corresponding neighbour sets and the estimation algorithms.

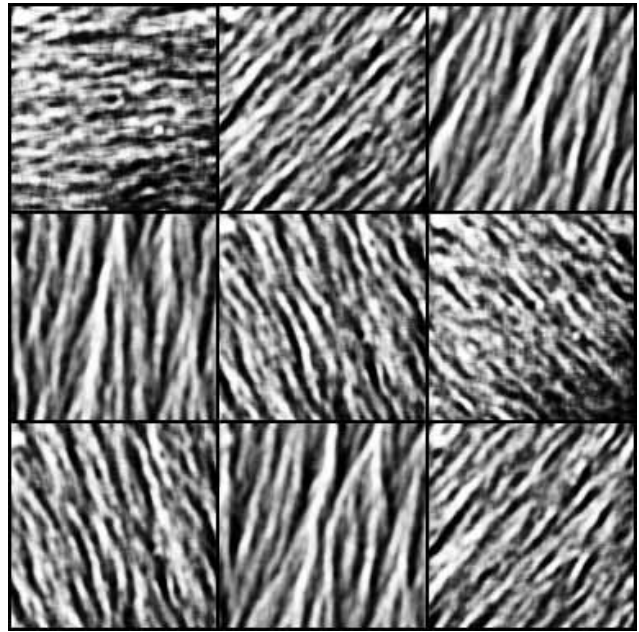


Figure 1: Original MM images

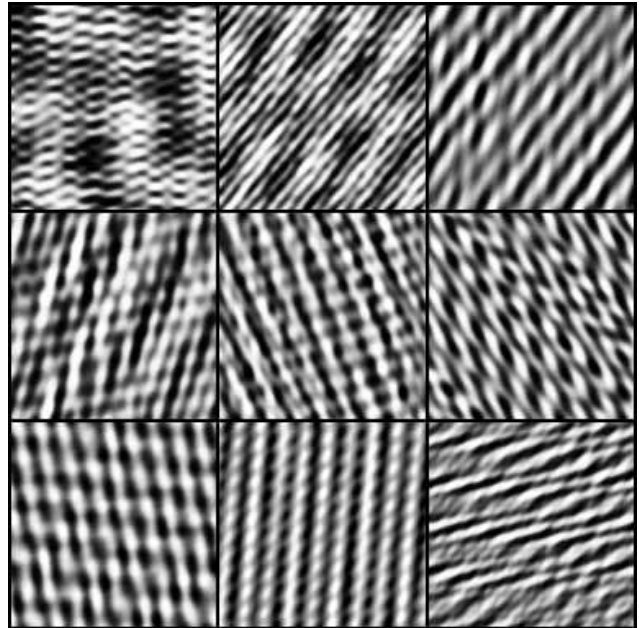


Figure 2: Top most ranked synthesised image per original. Windows (1,1), (1, 2), (1, 3), (2, 1), (2, 2), (2, 3), (3,1), (3,2) and (3,3) are images generated with a square-shaped neighbour set size of 13×13 (ML), 13×13 (LSQ), 7×7 (ML), 9×9 (ML), 5×5 (ML), 5×5 (LSQ), 3×3 (ML) and 9×9 (ML), respectively.

Although the synthesised images do reflect, to some extent, the basic visual properties of their corresponding originals, the overall

comparison of Figures 1 and 2 is not very convincing, even though some of the models involve many parameters. These results indicate that SAR models with symmetric neighbour sets are not good candidates for MM image synthesis.

5.2. Synthesis with Texture Orientation Neighbour Sets

To examine the effect of SAR models with non-symmetric neighbour sets, we used the neighbour sets $N_i, i = 1, 2, 3, \dots, 10$, shown in Fig. 3. These sets were selected based on the ripple direction and coarseness of the MM images, by the method of Section 3. For example, the shapes of neighbour sets N_1 and N_7 follow the 45° -diagonal direction that is the main orientation of the MM images of Figures 1(2,2) and (3,1), and the shapes of N_5 and N_9 approximately resemble the ripple shape of the MM images of Figures 1(2,1) and (3,2).

The SAR models with the above neighbour sets are fitted to the 9 real MM images, using both the LSQ and the ML algorithms. A total of $2 \times 10 \times 9 = 180$ synthesised images are, therefore, produced. Figure 4 presents the synthetic images using the neighbour sets given in Fig. 3, based on the original given in Fig. 1(2,2); for each neighbour set, we show only the better of the two images obtained using LSQ and ML. Generally speaking, the qualities of

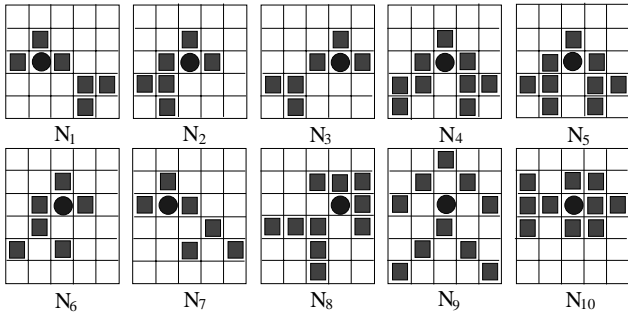


Figure 3: Neighbour set structures. The disk indicates the pixel of interest and the dark squares indicate the neighbour sets.

these images are much better than those obtained using symmetric sets. This is revealed in Table 1, which lists those neighbour sets that have led to the 5 best matched synthesised images for each original MM image, retrieved from an image base consisting of the 2×10 synthetic images with non-symmetric sets and the 10 synthetic images with symmetric sets. Amongst 45 (9×5) synthesised images represented in the table, only five were based on symmetric neighbour sets. Furthermore, the only one of them that was ranked first required many more neighbours than the one ranked second (84 as opposed to 10), whereas the qualities of these two synthesised images are actually very similar. The nine best synthesised images, one per original, are provided in Fig. 5; for the original of Fig. 1(1,1) the second ranked synthesised image is treated as the best for the above reason. In addition, even the less satisfactory synthesised images based on non-symmetric neighbour sets generally outperform those using the symmetric sets.

Collectively, the above results indicate that an SAR model is able to characterise the spatial interaction of the image grey levels along selected directions. In particular, the structure, i.e. both the shape and the size, of a neighbour set employed within the SAR model, plays a major role in the synthesis of MM images. Different

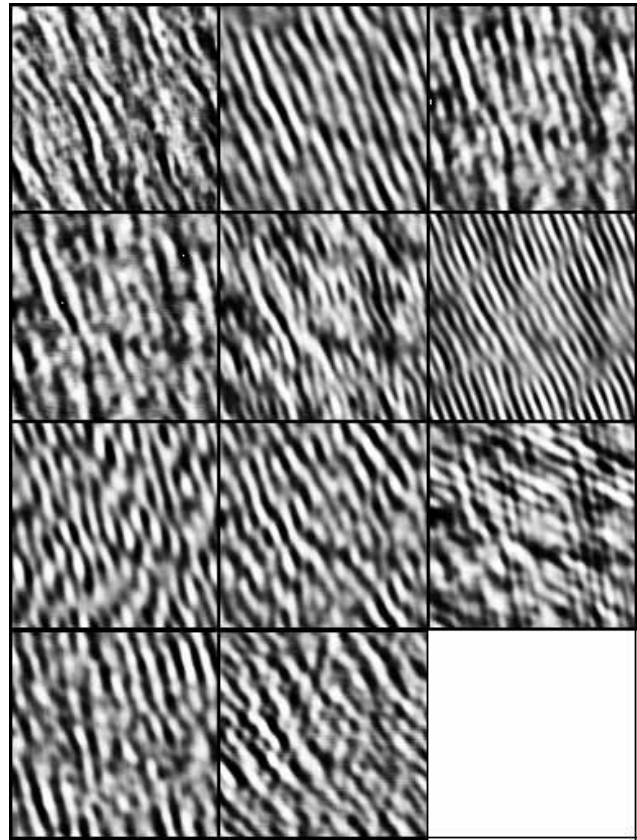


Figure 4: Original and synthesised images using neighbour sets given in Fig. 3. The original image is shown in window (1,1) and the synthesised images corresponding to the use of neighbour sets numbered from N_1 up to N_{10} are in raster-scan order.

Image		1st	2nd	3rd	4th	5th
Fig. 1 (1,1)	Set	13×13	N_8	7×7	N_6	N_{10}
	Algor.	ML	ML	ML	LSQ	ML
Fig. 1 (1,2)	Set	N_6	13×13	N_2	N_5	N_3
	Algor.	ML	LSQ	ML	LSQ	ML
Fig. 1 (1,3)	Set	N_1	N_5	N_1	N_{10}	N_9
	Algor.	ML	LSQ	LSQ	ML	ML
Fig. 1 (2,1)	Set	N_9	N_3	N_9	N_7	N_4
	Algor.	LSQ	ML	ML	ML	LSQ
Fig. 1 (2,2)	Set	N_1	N_1	5×5	N_4	9×9
	Algor.	ML	LSQ	ML	LSQ	ML
Fig. 1 (2,3)	Set	N_6	N_4	N_{10}	N_5	N_1
	Algor.	LSQ	LSQ	LSQ	LSQ	ML
Fig. 1 (3,1)	Set	N_1	N_1	N_4	N_5	N_7
	Algor.	ML	LSQ	LSQ	LSQ	LSQ
Fig. 1 (3,2)	Set	N_8	N_4	3×3	N_1	N_7
	Algor.	ML	LSQ	ML	ML	LSQ
Fig. 1 (3,3)	Set	N_3	N_2	N_3	N_6	N_6
	Algor.	ML	LSQ	LSQ	LSQ	ML

Table 1: Neighbour sets and algorithms corresponding to the top 5 synthesised images for each original

neighbour set structures capture different information embedded

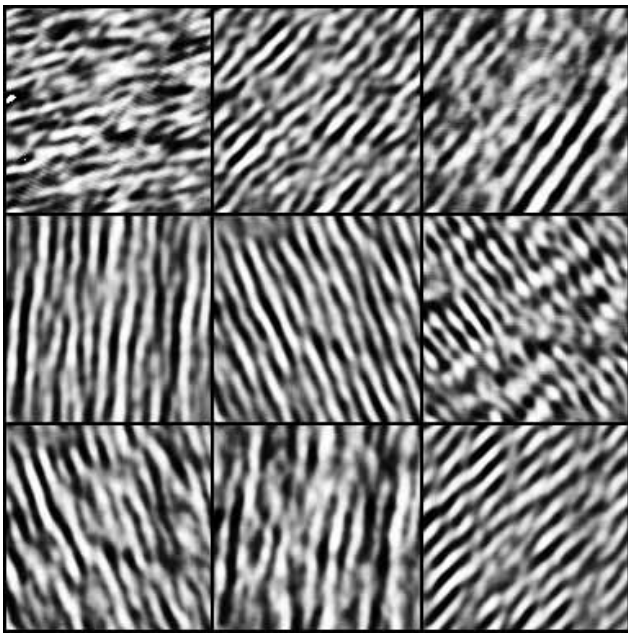


Figure 5: Top ranked synthesised image for each original. Windows (1,1), (1, 2), (1, 3), (2, 1), (2, 2), (2, 3), (3,1), (3,2) and (3,3) are images respectively generated with the following neighbour sets (and the associated estimation method): $N_8(\text{ML})$, $N_6(\text{ML})$, $N_1(\text{ML})$, $N_9(\text{LSQ})$, $N_1(\text{ML})$, $N_6(\text{LSQ})$, $N_1(\text{ML})$, $N_7(\text{ML})$ and $N_3(\text{ML})$.

in an original image; some structures are suitable for coarse textures while others for fine ones. A particular neighbour set should not be expected to suit a wide variety of textures, though certain structures may happen to be applicable for a number of different originals; see the appearance in Table 1 of set N_1 , whose orientation resembles those of Figures 1(1,3), (2,2) and (3,1). The choice of a neighbour set seems more important than the parameter estimation method, for our real images. Also, the size of a suitable non-symmetric set can be much smaller than that of the symmetric neighbour set required to achieve comparably good synthesis.

6. CONCLUSION

This paper has presented a new application of SAR models for the synthesis of textures which resemble real-life magnetic material images. The potential impact is examined of the structure of the neighbour set used in SAR models. The simulation results demonstrate that, with the use of a neighbour set structure mirroring the distinctive ripple in a given MM image, the resultant SAR model can accurately capture the essential characteristics of the image. This allows a synthetic image generated from such an SAR model to have very similar statistical and visual properties to its original. However, in general, the use of symmetric neighbour sets, even those of a moderately large size, typically results in synthesised images of a poor quality. In our future work we shall pursue the possible implications of this modelling for the understanding and representation of the underlying magnetic phenomena.

7. REFERENCES

- [1] R. Chellappa, S. Chatterjee and R. Bagdazian. Texture synthesis and compression using Gaussian-Markov random field models. *IEEE Trans. on Systems, Man, and Cybernetics*, SMC-15(2):298–303, 1985.
- [2] R. C. Gonzalez. *Digital Image Processing*. Addison-Wesley Company, 1984.
- [3] D. J. Hand. *Discrimination and classification*. Hohn Wiley and Son Ltd, 1981.
- [4] R. L. Kashyap and R. Chellappa. Estimation and choice of neighbors in spatial-interaction models of images. *IEEE Trans. on Information Theory*, IT-29(1):60–72, 1983.
- [5] J. M. Keller and R. M. Cownover. Texture description and segmentation through fractal geometry. *Comput. Vision Graphics Image Process.*, 45:150–166, 1989.
- [6] A. Khotanzad and R. L. Kashyap. Feature selection for texture recognition based on image synthesis. *IEEE Trans. on Systems, Man, and Cybernetics*, SMC-17(6):1087–1095, 1987.
- [7] J. P. King, J. N. Chapman, J. C. S. Kools and M F Gillies. On the free layer reversal mechanism of FeMn-biased spin-valves with parallel anisotropy. 1998. Submitted to *J. Phys. D: Appl. Phys.*
- [8] F. Liu and R. W. Picard. Periodicity, directionality, and randomness: wold features for image modelling and retrieval. *IEEE Trans. on Pattern Analysis and Machine Intelligence*, PAMI-18(7):722–733, 1996.
- [9] B. Manjunath and W. Ma. Texture features for browsing and retrieval of image data. *IEEE Trans. on Pattern Analysis and Machine Intelligence*, PAMI-18(8):837–842, 1996.
- [10] J. Mao and A. K. Jain. Texture classification and segmentation using multiresolution simultaneous autoregressive models. *Pattern Recognition*, 25(2):173–188, 1992.
- [11] W. Qian and D. M. Titterton. Bayesian image restoration: An application to edge-preserving surface recovery. *IEEE Trans. on Pattern Analysis and Machine Intelligence*, PAMI-15(7):748–752, 1993.
- [12] A. Speis and G. Healey. An analytical and experimental study of the performance of markov random fields applied to texture images using small samples. *IEEE Trans. on Image Processing*, IP-5(3):447–458, 1996.
- [13] J. K. Tugnait. Estimation of linear parametric models of non-gaussian discrete random fields with application to texture synthesis. *IEEE Trans. on Image Processing*, IP-3(2):109–127, 1994.